

Pair dispersion in a chaotic flow reveals the role of the memory of initial velocity

Eldad Afik* and Victor Steinberg

Department of Physics of Complex Systems, Weizmann Institute of Science,
Rehovot 76100, Israel

Abstract

The leading paradigm for chaotic flows dominated by dissipation predicts an exponential growth of the mean distance between pairs of fluid elements, in the long run. This is reflected in the analysis of experimental results on tracer particles and the discussions which follow, as reported in recent experimental and numerical publications. To quantitatively validate this prediction, we have conducted a microfluidic experiment generating *elastic turbulence*, a flow characterised in the literature as smooth in space and random in time. To our great surprise, we discovered that the pair separation follows a much slower power-law — also known as *ballistic* — a notion overlooked so far for flows of this type. We provide conclusive experimental evidence that this scaling is well-described by the same coefficients derived from the short-time dynamics. Our finding reinforces the role of the ballistic regime over a significant range in time and space, providing a quantitative estimation for the spreading of particles in mixing microfluidic flows based on the initial velocity snapshot. Finally we note that the conditions for the asymptotic exponential pair separation are quite stringent when it comes to tracer particles and are unlikely to be realised in wall-bounded flows. Therefore this work raises questions regarding the relevance and applicability of the currently leading paradigm.

Keywords. chaotic flows | pair dispersion | microfluidic | fluid dynamics | elastic turbulence

When we stir sugar in a cup of coffee we typically drive the liquid in circles using the tea-spoon, yet the flow quickly evolves into a three-dimensional chaotic one, tremendously accelerating the homogeneous distribution of the sweetener throughout the beverage. Turbulent flows, typical in our everyday life, are renowned for their efficient mixing and intensification of particle dispersion, having impact on natural processes as well as wide applications in the industry [1]. At their smaller scales — the so-called dissipative or Kolomogorov scales — such flows are characterised by a velocity field which is smooth in space yet fluctuates strongly in time, also known as the *Batchelor regime* [2].

Understanding transport phenomena at small scales is of importance for the study of combustion, contamination and the deformation of polymers by the flow [3], to name but a few physical examples, as well as for the study of biological processes such as cytoplasmic streaming [4], communication via chemo-attractants and food searching [5]. Moreover, it has immediate technological implications, mainly when it comes to miniature devices. Microfluidic systems have become a common tool in research and industry. As a prominent part of lab-on-a-chip apparatuses, they are

*To whom correspondence should be addressed; email: eldad.afik@weizmann.ac.il

implemented for micro-chemistry [6, 7], soft condensed matter [8], bioanalytics such as PCR [9, 10], biomedicine and other research and engineering applications [11]. Nevertheless, there is limited knowledge of transport phenomena in these devices beyond the scenario of laminar steady flows, which is not the only case of interest [8, 12, 6].

The study of particle dispersion in flows is at the basis of the understanding of transport processes [2, 1, 3]. In the early 1950s, G. K. Batchelor predicted that the mean length of material lines in turbulent flows would grow exponentially in the course of time, in the long time limit; this stems from the notion that the line elements it consists of can be considered short enough such that the distance between the ends of an element remain within the dissipative scale throughout the motion [13, 14]. In some recent works the terms *material line* and *material line element* are used interchangeably to indicate the separation vector between two passive particles in the fluid [15, 16, 3]. And indeed Batchelor’s prediction has been later reformulated for tracer particles in the form of exponential pair separation; see [3, §2] for example. To illustrate how this comes about, let us consider a pair of passive tracers separated by the vector \mathbf{R} , and whose relative velocity is \mathbf{u} . The evolution of the squared separation distance R^2 follows

$$\frac{1}{2} \frac{d}{dt} R^2 = \mathbf{u} \cdot \mathbf{R} = u_l R , \quad (1)$$

where u_l is the separation velocity, defined by the above relation. The analysis then proceeds by assuming a linear flow approximation — the pair separation is considered to be small enough such that the velocity of one tracer is linearly related to that of the other. Using this approximation Eq. 1 reduces to

$$\frac{1}{2} \frac{d}{dt} R^2 = \xi R^2 , \quad (2)$$

where ξ no longer depends on R . For the case of chaotic flows, ξ can be modelled as a random variable, and analyses often focus on the expectation value of such equations [14, 2, 3]. Additionally assuming the correlation time of ξ to be very short compared to the observation time [2, 3], a generalisation of the central limit theorem – the multiplicative ergodic theorem of Oseledec [2, 17] – is applied, resulting in the exponential pair dispersion

$$\langle R(t)^2 \rangle = R^2(t_0) \exp \left\{ 2\tilde{\xi} (t - t_0) \right\} . \quad (3)$$

This is a relation for the time evolution of the second moment of pair separation distances. In this form one can identify $2\tilde{\xi}$ with the generalised Lyapunov exponent of the second order, which is generically not trivially related to the ordinary (maximal) Lyapunov exponent; see [18, §3.2.1], [17, §5.3], [2] and others.

Much of the theoretical and numerical literature discussing pair dispersion in the dissipative sub-range is devoted to the evaluation of $\tilde{\xi}$ in terms of the typical time-scale of the flow τ , that is $\tilde{\xi} = \gamma/\tau$; see [13, Eq. 2.9]. The value of γ is still under debate as can be learnt from [14, §24.5] as well as [3] and references therein.

At the time of writing, the exponential pair dispersion is regarded as the leading paradigm for chaotic flows which are spatially smooth, as manifested by the analysis of recent experimental results and the discussions which follow. Jullien [19] studied an instance of the Batchelor regime flow in 2d turbulence, where the velocity field was inferred experimentally followed by numerical integration of tracers simulated on a computer; an exponential separation, referred to in that context as Lin’s law [20], was reported during an intermediate time interval of between one to twice the value of the

estimated τ , after which a power-law scaling has been observed. Salazar and Collins [3] estimated γ from measurements of $\langle \xi \rangle$ in 3d turbulence reported by Guala et al. [16]; this estimate should be taken with grain of salt not only because it is unclear whether these measurements are indeed restricted to the dissipative scales but also as, although related, the quantities $\langle \xi \rangle$ and $\tilde{\xi}$ are not the same [14]. Even more recently, Ni and Xia [21] reported measurements in 3d turbulent thermal convection and inferred γ from exponential fits to the mean squared pair separation distance; as presented in [21, Fig. 1], the fits are taken at time intervals of up to one Kolmogorov time-scale, a time too short with respect to the underlying assumptions, and thereafter the data grows faster than the evaluated exponentials. We therefore find it safe to conclude that the literature on the subject is lacking conclusive experimental evidence.

In this paper we report experimental results of particle pair dispersion where, in contrast to the above mentioned publications [19, 3, 21], the memory of the initial relative velocity prevails the dynamics, showing no signature of the asymptotic exponential growth.

Studying pair separation in the dissipative sub-range over long times in intense turbulence poses a technological challenge. The high velocities, typical of high Reynolds flows, restrict the length of the obtained trajectories as exemplified by the above mentioned reports [19, 15, 21] and other recent works [22]. This is one of the reasons for which the experimental literature on pair dispersion in smooth chaotic flows is lagging behind the theoretical one.

However, chaotic flows do not necessarily require fast velocities or large vessels. One might expect viscous flows to be regular in microfluidic tubes and the question of mixing in these apparatuses may seem irrelevant due to their low Reynolds nature. Nevertheless, when a minute amount of long flexible polymers, such as DNA and protein filaments, are introduced, the flow may develop a series of elastic instabilities which render it irregular and twisted, a phenomenon termed *elastic turbulence* [23, 8, 24].

The study of pair separation dynamics in elastic turbulence, taking place inside a tiny tube, presents technical challenges: (i) The positions of tracers are needed to be resolved over long times and distances, in particular when the tracers get nearby to each other, whereas the flow is chaotic and three-dimensional; (ii) The scales at which the dynamics takes place require the use of a microscope, where 3d imaging is non-trivial; (iii) The flow fluctuations in time dictate a high temporal resolution; (iv) The statistical nature of the problem demands a large sample of trajectories, which in turn requires long acquisition times and reliable automation. To satisfy these requirements a novel method was implemented. The 3d positions of the fluorescent particles are determined from a single camera 2d imaging, by measuring the diffraction rings generated by the out-of-focus particle; this way the particle localisation problem turns into a ring detection problem, which is addressed accurately and efficiently in Ref. [25].

Below we report the results of an experiment designed to measure the value of γ using direct Lagrangian particle tracking in an elastic turbulence flow in a microfluidic tube.

Results

We have established an experimental database of trajectories derived from tracers in the flow; see Materials and Methods. One example of a pair realisation can be found in Fig. 1A,B. A sub-sample of pair separation $\mathbf{R}(\delta t)$ curves is plotted in Fig. 1C; here $\delta t = t - t_0$ and $\mathbf{R}_0 = \mathbf{R}(\delta t = 0)$. These curves, together with the rest of the pairs which were found in each R_0 bin, were collected and the second moments were calculated to construct the datasets of $\langle (R(\delta t)/R_0)^2 \rangle_{R_0}$ presented

in Fig. 2 on a semi-logarithmic scale, where an exponential curve would have appeared linear (the un-normalised data $\langle R^2(\delta t) \rangle_{R_0}$ can be found in Fig. S7; the sample size data is presented in Fig. S8).

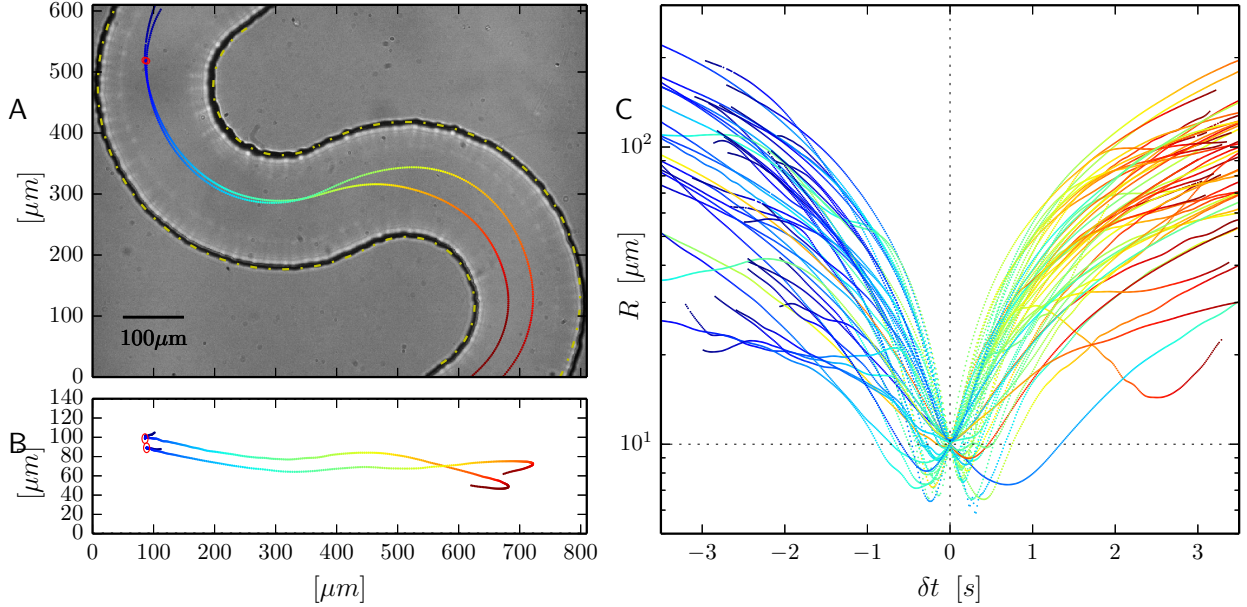


Figure 1: **Pair dynamics example.** The trajectories of two tracers are plotted in the left panels. The right panel shows a sub-sample of pair separation distances in the course of time. The figure demonstrates the chaotic nature of the flow as manifested by pairs, and outlines the analysis forming the ensembles of pairs. (A) A projection on to the camera plane, overlaid on a bright field image of the observation window (further technical details are provided in Fig. S1 and in the Materials and Methods). (B) A side projection. For the sake of visualisation the vertical axis is stretched by 3/2. All pairs of tracers which were detected at some instant at a prescribed separation distance, $R_0 = 10 \pm 0.5 \mu\text{m}$ in this example, are collected to form one ensemble. The event at which the pair separation was nearest to R_0 , marked by the red circles in the plot, is recorded as t_0 for the particular pair for later analysis. The colour code in the plot denotes time, which spans 4s in this case. (C) A sub-sample of pair separation distance trajectories $R(\delta t)$ for pairs belonging to the $R_0 = 10 \mu\text{m}$ ensemble, presented on a semi-logarithmic scale; For each pair, $\delta t = t - t_0$ is the time elapsed since t_0 . The colour code denotes time, scaled separately for each curve. The plot shows a sub-sample of 49 pairs out of more than 4×10^4 pairs in this ensemble; see Fig. S8 for sample size data.

However, our data shows no supporting evidence for the predicted exponential growth of the second moment of pair separations. The insets present a zoom-in on the temporal sub-intervals where the full range plot may seem to contain linear segments. Nevertheless, no single slope, to be identified with $2\tilde{\xi}$ in Eq. 3, can be found. Moreover, an exponential pair dispersion should extrapolate to the origin on this plot, and this is clearly not the case.

To our great surprise we have found that, for a significant fraction of the observation time, the mean relative pair dispersion evolves quadratically in time to leading order $\langle \|\mathbf{R}(\delta t) - \mathbf{R}_0\|^2 \rangle \propto \delta t^2$; this observation is evident in the insets of Fig. 3, and stands in sharp contradiction to the interpretations of recent experimental results [19, 3, 21]. To better understand the source for this scaling let us write the Taylor expansion around $\delta t = 0$

$$\mathbf{R}(\delta t) = \mathbf{R}_0 + \mathbf{u}_0 \delta t + \frac{1}{2} \dot{\mathbf{u}}_0 \delta t^2 + \mathcal{O}(\delta t^3) . \quad (4)$$

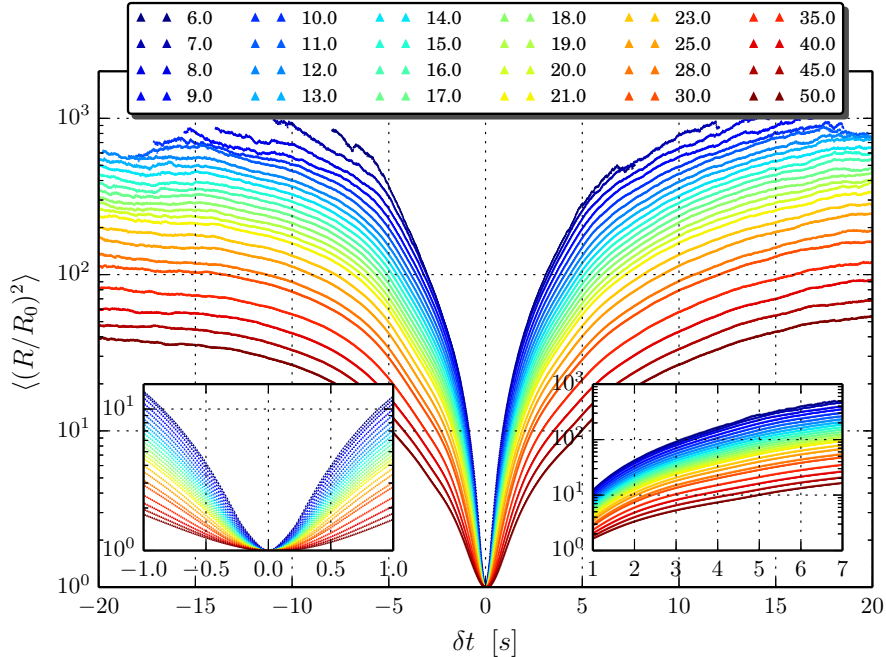


Figure 2: **Pair dispersion normalised by the initial separation.** The plot shows the average squared pair separation distance, normalised by the initial separation, $\langle (R(\delta t)/R_0)^2 \rangle_{R_0}$ for various R_0 between 6 and 50 μm ; The insets show a zoom-in on the initial and intermediate time intervals. The data shows no supporting evidence for the exponential time dependence which follows from Eq. 3.

Substituting this in the expression for the relative pair dispersion and considering the ensemble average over pairs of the same initial separation

$$\langle \|\mathbf{R}(\delta t) - \mathbf{R}_0\|^2 \rangle_{R_0} = \langle u^2 \rangle_{R_0, t_0} \delta t^2 + \langle \dot{\mathbf{u}} \cdot \mathbf{u} \rangle_{R_0, t_0} \delta t^3 + \mathcal{O}(\delta t^4), \quad (5)$$

we find that the leading order term at short times is indeed quadratic in δt — the so-called *ballistic* regime.

This is a universal property which does not require any assumptions on the character of the flow. A sign of this scaling beneath the dissipative scale has been observed in simulations of isotropic turbulence [26, Fig. 5]. Yet neither quantitative analysis of the coefficients in Eq. 5 nor any contrast with the exponential separation prediction were made. Other experimental [27] and numerical [26, 28] results are limited to the inertial subrange of turbulence.

To test this further we rescale the relative pair dispersion by the pre-factor, the mean initial squared relative velocity $\langle u^2 \rangle_{R_0, t_0}$. Unlike the case of inertial turbulence, for elastic turbulence there are no exact results nor scaling arguments to derive the coefficients appearing in Eq. 5. Therefore we extract them from the experimental data; the $\langle u^2 \rangle_{R_0, t_0}$ profile as function of R_0 is presented in Fig. S2A. Indeed we find that our data admits a scaling collapse with no fitting parameters, providing a convincing experimental evidence that these observations are well-described by the short time expansion of the relative pair dispersion. The data shown in Fig. 3 seem to deviate significantly from the quadratic scaling only after 2–3 seconds.

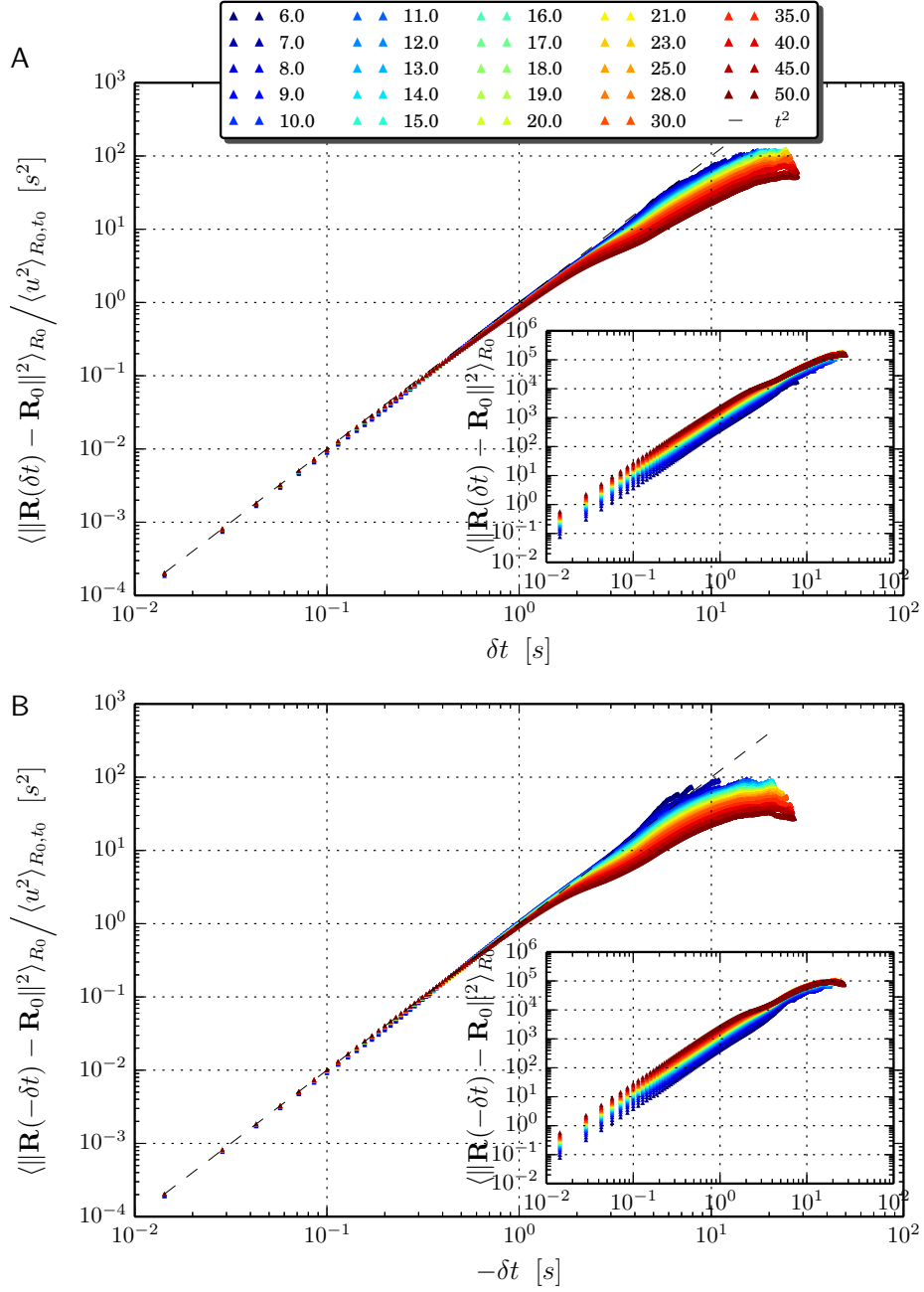


Figure 3: **Relative pair dispersion.**

(A) Forward in time $\langle \|\mathbf{R}(\delta t) - \mathbf{R}_0\|^2 \rangle_{R_0}$ for various initial separations (inset) between 6 and 50 μm , collapse initially on a single curve which follows a power-law δt^2 , once rescaled by the average squared relative velocity at the initial time, $\langle u^2 \rangle_{R_0, t_0}$. A significant deviation from δt^2 is noticed after 2–3 s, indicating the time beyond which higher order terms should be considered. (B) Backwards in time relative pair dispersion $\langle \|\mathbf{R}(-\delta t) - \mathbf{R}_0\|^2 \rangle_{R_0}$ for the same initial separations (inset), showing the same initial scaling collapse as the forward in time.

In order to expose the sub-leading contributions to the initial relative pair dispersion, we subtract the backwards-in-time dynamics from the forward one. This way the time-symmetric terms, even powers of δt , are eliminated. The result, the time asymmetric contributions presented in Fig. 4, shows that indeed initially the next-to-leading order correction follows δt^3 and that the curves do collapse onto one when rescaled by $\langle \dot{\mathbf{u}} \cdot \mathbf{u} \rangle$, the appropriate coefficient in Eq. 5. The values of $\langle \dot{\mathbf{u}} \cdot \mathbf{u} \rangle_{R_0, t_0}$ were, once again, extracted from the experimental data; see Fig. S4 for the R_0 profile. However, the deviations from this scaling are noticeable earlier than half a second, much earlier than the deviations from the ballistic behaviour discussed above. This hints that the deviation observed in Fig. 3 is in fact due to higher order terms, potentially an indication of a transition to another regime. The fact that the transition takes place at an earlier time for the larger initial separations indicates the potential effects of the vessel size and its geometry, as well as the failure of the linear flow approximation; see Fig. S2.

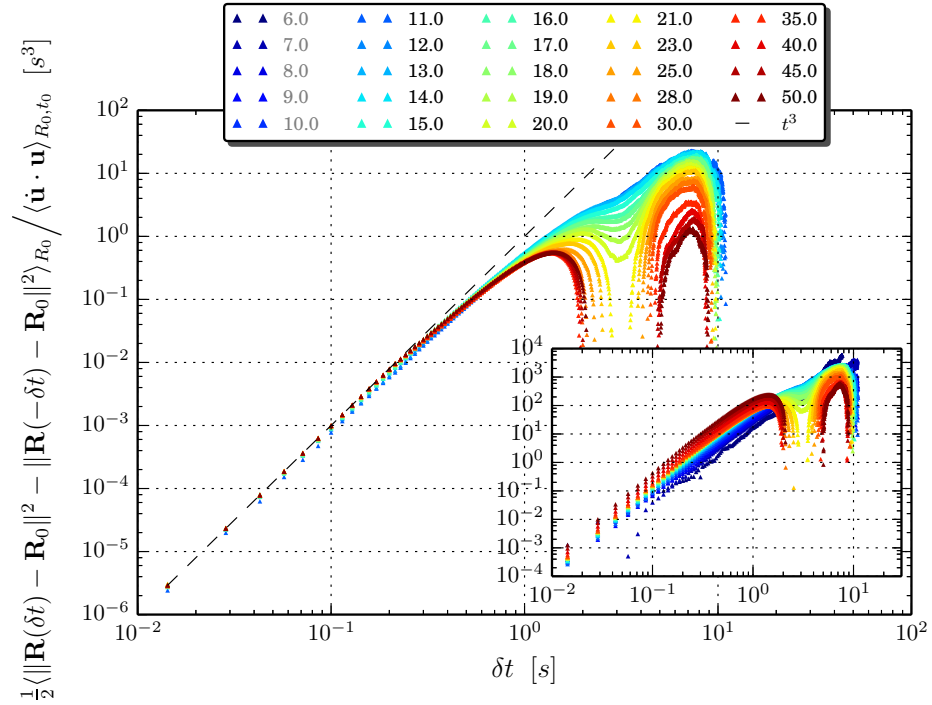


Figure 4: **Time asymmetric contribution to the relative pair dispersion.** Taking the difference between the datasets presented in the insets of Fig. 3, $\frac{1}{2} \langle \|\mathbf{R}(\delta t) - \mathbf{R}_0\|^2 - \|\mathbf{R}(-\delta t) - \mathbf{R}_0\|^2 \rangle_{R_0}$ exposes the contribution of the time-asymmetric elements (odd powers in δt), shown in the inset (after sign inversion). These data collapse on a single curve which follows δt^3 when rescaled by $\langle \dot{\mathbf{u}} \cdot \mathbf{u} \rangle_{R_0, t_0}$. The datasets of $R_0 \leq 10 \mu\text{m}$ (grey in the legend) are omitted from the main figure due to the scatter of the estimator (see Fig. S4). The plot shows a deviation from δt^3 scaling at times shorter than 400 ms, indicating the dominance of higher order (odd) terms at early times and that the δt^3 term alone does not trivially explain the deviation from δt^2 , observed in Fig. 3.

Discussion

In the light of Eq. 5, the ballistic evolution at short times should not be too surprising. And yet, to our knowledge it has not been discussed experimentally, nor confronted with the exponential separation prediction. Moreover, the ‘memory’ of the initial conditions in our data is longer than one may have expected. On the one hand, our observations are consistent with the time-scale δt^* derived from the ratio of the coefficients in Eq. 5 (see Fig. S5), as deviations from the δt^2 scaling are expected to be noticeable for $\delta t \leq 0.1\delta t^*$. This is also manifested in the rescaling of the data by δt^* , presented in Fig. S6, and to be compared with numerical simulations of inertial turbulence [28, Fig. 1]. On the other hand, during the time the statistics are dominated by the initial conditions, single realisations are not monotonic nor predictable (see Fig. 1), that is to say, our observations are not a trivial result of the mean flow alone, which in itself is inhomogeneous. Moreover, during one second tracers typically travel distances larger than the width of the tube. Given the stochastic nature of the dynamics, the spatial structure of the flow and the limited range of the linear flow approximation (see insets in Fig. S2), the Taylor expansion in time Eq. 5 was expected to have a rather restrictive radius of convergence. Further analysis is required to clarify whether higher order terms are of importance and to estimate the Lagrangian correlation time, which accounts for both the temporal and the spatial structure of the flow. Hence, in-depth discussion of the transition away from the ballistic regime in our system is left for future work.

Nonetheless, the time for which the ballistic approximation holds is longer than a second, a memory of the initial relative velocities which allows a wide prediction horizon. We are unaware of any previous discussion of pair dispersion short time statistics neither in the context of elastic turbulence nor for the broader class of wall-bounded viscous mixing flows. The implications are far-reaching — knowing the average velocity difference at a given scale, which is an Eulerian property, one can determine the degree of dispersion, a Lagrangian property, as was recently discussed in [29]. We have demonstrated its predictive power over a significant time interval, which provides a new paradigm for chaotic flows dominated by dissipation.

The exponential growth in Eq. 3 relies on two underlying assumptions [13, 2, 3]: (i) the velocity field admits a linear approximation in space throughout the observation time; and (ii) the observation time is much longer than the correlation time of the velocity gradients. These requirements are quite stringent and are not fulfilled by our experiment. To the best of our knowledge these assumptions have not been met experimentally for tracer particles so far, and yet the exponential growth prediction seems to be the leading paradigm in interpreting experimental results [19, 3, 21]. Our estimations for the experimental system presented here indicate these may be possibly relevant for $R_0 \lesssim 0.1 \mu\text{m}$ and $\delta t \gtrsim 10 \text{s}$. Examining the experimental parameters reported in recent works [1, 27, 22] we find that the trade-off between short correlation times and a large enough dissipation scale renders them difficult to reach in intense inertial turbulence, as Batchelor himself anticipated [13, §1]; also see [14, §24.5].

The lesson in this case highlights the limitations of asymptotic analyses for the descriptions of real-world flows — for practical purposes the asymptotic dynamics are not necessarily the generic description which should be considered but rather the short-time behaviour, here dictated by the Eulerian averages at the initial time. According to our findings the Lyapunov exponents picture is not the appropriate one to describe the dynamics of wall-bounded elastic turbulence at scales larger than few percent of the vessel size. This raises questions regarding the mechanism for polymer stretching once their end-to-end distance reaches few microns length.

Following our work one may reach the conclusion that the Batchelor prediction [13] is irrelevant.

By all means, this is not the case! Batchelor considered the evolution of the total length of a material line while this work, like the above mentioned reports [19, 3, 21], focused on the shortest distance between pairs of tracers starting with a finite initial separation. Therefore the question of what natural or experimental systems admit the assumptions underlying the exponential pair dispersion Eq. 3 for tracer particles persists.

Materials and methods

Methods Summary The work presented here relies on constructing a database of trajectories in an elastic turbulence flow. Elastic turbulence is essentially a low Reynolds number and a high Weissenberg number phenomenon. The former means the inertial non-linearity of the flow is overdamped by the viscous dissipation. The latter estimates how dominant is the non-linear coupling of the elastic stresses to the spatial gradients of the velocity field compared with the dissipation of these stresses via relaxation. This is the leading consideration in the design of the flow cell.

The Lagrangian trajectories are inferred from passive tracers seeded in the fluid. In order to study the dynamics of pairs, the 3d positions of the tracers are needed to be resolved, even when tracers get nearby to each other. The requirement of large sample statistics dictates the long duration of the experiment, which lasts over days. The fluctuations due to the chaotic nature of the flow set the temporal resolution at milliseconds. This leads to a data generation rate of about 180 GB/h. Hence both the acquisition and the analysis processes are required to be steady and fully automated. The 3d positions of the fluorescent particles are determined using 2d single camera imaging, by measuring the diffraction rings generated by the out-of-focus particle. This way the particle localisation problem turns into a ring detection problem [25].

Microfluidic apparatus The experiments were conducted in a microfluidic device, implemented in polydimethylsiloxane elastomer by soft lithography, consisting of a curvilinear tube having a rectangular cross-section. The depth is measured to be 140 μm , the width is approximately 185 μm (see Fig. S1). The geometry consists of a concatenation of 33 co-centric pairs of half circles. The working fluid consists of polyacrylamide ($\text{MW}=1.8 \times 10^7$ Da at mass fraction of 80 parts per million) in aqueous sugar syrup (1:2 sucrose to d-sorbitol ratio; mass fraction of 78%), seeded with fluorescent particles (1 micron Fluoresbrite YG Carboxylate particles, PolySciences Inc.) at number density of about 50 tracers in the observation volume. The viscosity of the Newtonian solvent, without the polymers, is estimated to be 1100 times larger than water viscosity at 22 $^\circ\text{C}$. This leads to a polymer longest relaxation time of $\tau_p \simeq 100$ s [30], which is the longest time scale characterising the relaxation of elastic stresses in the solution. The flow was driven by gravity. The maximal time-averaged velocity was measured to be roughly $v_{\text{max}} \simeq 250$ $\mu\text{m}/\text{s}$. This results in a Reynolds number $Re \lesssim 10^{-4}$ and a global Weissenberg number $Wi = \tau_p \frac{v_{\text{max}}}{\text{width}/2} \gtrsim 250$.

Imaging system The imaging system consists of an inverted fluorescence microscope (IMT-2, Olympus), mounted with a Plan-Apochromat 20 \times /0.8NA objective (Carl Zeiss) and a fluorescence filter cube; a Royal-Blue LED (Luxeonstar) served for the fluorophore excitation. A CCD (GX1920, Allied Vision Technologies) was mounted via zoom and 0.1 \times c-mount adapters (Vario-Orthomate 543513 and 543431, Leitz), sampling at 70 Hz, 968 px \times 728 px, covering 810 μm \times 610 μm laterally and the full depth of the tube. The camera control was based on a modification of the Motmot Python camera interface package [31], expanded with a home-made plug-in, to allow real-time

image analysis in the RAM [25], recording only the time-lapse positions of the tracers to the hard drive.

Lagrangian particle tracking To construct trajectories, the particle localisation procedure, introduced in [25], has to be complemented by a linking algorithm. Here we implemented a kinematic model, in which future positions are inferred from the already linked past positions. We used the code accompanying [32] as a starting point. The algorithm was rewritten in Python [33], generalised to n-dimensions, the kinematic model modified to account for accelerations as well, a memory feature was added to account for the occasional loss of tracers, and it was optimised for better performance. The procedure accounts for the physical process of particles advected by a smooth chaotic flow and for the uncertainties. These arise from the chaotic in time nature of the flow (“physical noise”) as well as from localisation and past linking errors (“experimental noise”). Finally, natural smoothing cubic splines are applied to smooth-out the experimental noise and estimate the velocities and accelerations [34, 35]. The smoothing parameter is chosen automatically, where Vapnik’s measure plays the role of the usual generalised cross-validation, adapted from the Octave splines package [36].

Pairs analysis Within the trajectories database we have identified pairs of tracers which were found at some instant at a separation distance close to a prescribed initial separation $R_0 = 6, 7, \dots, 50 \mu\text{m}$, to within $\delta R_0 = \pm 0.5 \mu\text{m}$. The initial time t_0 for a trajectory was set by the instant at which the separation distance was closest to R_0 . This way, each pair separation trajectory $R(\delta t)$ can contribute to an R_0 pairs ensemble at most once. See Fig. 1. The number of pairs considered in each R_0 ensemble is plotted in Fig. S8 as function of δt .

Examining the ensemble averages of the relative separation velocity at the initial time $\langle u_l \rangle_{R_0, t_0}$, presented in Fig. S3, we do not find an indication that our sampling method introduces a bias for converging or diverging trajectories, at least for $R_0 \lesssim 22 \mu\text{m}$. Such a bias could manifest itself in non-vanishing relative separation velocity at these scales. We have yet to resolve the reason for the negative values observed at the larger scales.

Our data supports the linear flow approximation assumption at small enough scales, as indicated by the ensemble averages of the initial relative separation velocity; see the inset of Fig. S2B where $\langle u_l^2 \rangle_{R_0, t_0} / R_0^2$ levels-off at $R_0 \lesssim 12 \mu\text{m}$. The same regime is not reached for the relative velocity, yet the data in the inset of Fig. S2A does not rule out this possibility for smaller scales.

One note of warning should be made as to the potential limitations when inferring the Eulerian mean squared relative velocity from direct Lagrangian particle trajectories, e.g. using $\langle u^2 \rangle_{R_0, t_0}$ in Fig. S2 as an estimator for the Eulerian second order structure function. The tracer number density in our experiment sets the mean separation distance to a value which is larger than the initial separations considered in this work. The analysis of the possible consequences are beyond the scope of this report. Yet we have no evidence for a discrepancy in the quantities we have considered here.

Acknowledgements We thank A. Frishman for the helpful and extensive discussions of the theory, O. Hirschberg for useful discussions of the mathematical and statistical analysis, M. Feldman for his insights regarding the implications to Biology, and Y. Silberberg for his helpful advices. EA

had fruitful discussions with J. Bec, S. Musacchio, D. Vincenzi, EW Saw and R. Chetrite, kindly organised by the latter; both authors gained from discussions with V. Lebedev and G. Falkovich. This work is supported by the Lower Saxony Ministry of Science and Culture Cooperation (Germany).

References

- [1] M. Bourgoin, N. T. Ouellette, H. Xu, J. Berg, and E. Bodenschatz. [The role of pair dispersion in turbulent flow](#). *Science*, 311(5762):835–838, Feb 2006.
- [2] G. Falkovich, K. Gawędzki, and M. Vergassola. [Particles and fields in fluid turbulence](#). *Rev. Mod. Phys.*, 73(4):913–975, Nov 2001.
- [3] J. P. Salazar and L. R. Collins. [Two-particle dispersion in isotropic turbulent flows](#). *Annual Review of Fluid Mechanics*, 41(1):405–432, Jan 2009.
- [4] F. G. Woodhouse and R. E. Goldstein. [Cytoplasmic streaming in plant cells emerges naturally by microfilament self-organization](#). *Proceedings of the National Academy of Sciences*, 110(35):14132–14137, Aug 2013.
- [5] A. Celani and M. Vergassola. [Bacterial strategies for chemotaxis response](#). *Proceedings of the National Academy of Sciences*, 107(4):1391–1396, Jan 2010.
- [6] A. J. deMello. [Control and detection of chemical reactions in microfluidic systems](#). *Nature*, 442(7101):394–402, Jul 2006.
- [7] J. P. McMullen and K. F. Jensen. [Integrated microreactors for reaction automation: New approaches to reaction development](#). *Annual Review of Analytical Chemistry*, 3(1):19–42, Jun 2010.
- [8] A. Groisman and V. Steinberg. [Efficient mixing at low reynolds numbers using polymer additives](#). *Nature*, 410(6831):905–908, Apr 2001.
- [9] J. Khandurina, T. E. McKnight, S. C. Jacobson, L. C. Waters, R. S. Foote, and J. M. Ramsey. [Integrated system for rapid PCR-based DNA analysis in microfluidic devices](#). *Analytical Chemistry*, 72(13):2995–3000, Jul 2000.
- [10] C. Zhang, J. Xu, W. Ma, and W. Zheng. [PCR microfluidic devices for DNA amplification](#). *Biotechnology Advances*, 24(3):243–284, May 2006.
- [11] E. K. Sackmann, A. L. Fulton, and D. J. Beebe. [The present and future role of microfluidics in biomedical research](#). *Nature*, 507(7491):181–189, Mar 2014.
- [12] A. D. Stroock, S. K. W. Dertinger, A. Ajdari, I. Mezi, H. A. Stone, and G. M. Whitesides. [Chaotic mixer for microchannels](#). *Science*, 295(5555):647–651, Jan 2002.
- [13] G. K. Batchelor. [The effect of homogeneous turbulence on material lines and surfaces](#). *Proceedings of the Royal Society A: Mathematical, Physical and Engineering Sciences*, 213(1114):349–366, Jul 1952.

- [14] A. S. Monin and A. M. Yaglom. *Statistical Fluid Mechanics, Volume II: Mechanics of Turbulence (Dover Books on Physics)*, volume 2. Dover Publications, 2007.
- [15] B. Lüthi, A. Tsinober, and W. Kinzelbach. [Lagrangian measurement of vorticity dynamics in turbulent flow](#). *J. Fluid Mech.*, 528:87–118, 2005.
- [16] M. Guala, B. Lüthi, A. Liberzon, A. Tsinober, and W. Kinzelbach. [On the evolution of material lines and vorticity in homogeneous turbulence](#). *J. Fluid Mech.*, 533, Jun 2005.
- [17] M. Cencini, F. Cecconi, and A. Vulpiani. *Chaos: From Simple Models to Complex Systems*. Series on advances in statistical mechanics. World Scientific, 2010.
- [18] G. Paladin and A. Vulpiani. [Anomalous scaling laws in multifractal objects](#). *Physics Reports*, 156(4):147225, Dec 1987.
- [19] M.-C. Jullien. [Dispersion of passive tracers in the direct enstrophy cascade: Experimental observations](#). *Physics of Fluids*, 15(8):2228, 2003.
- [20] J.-T. Lin. [Relative dispersion in the enstrophy-cascading inertial range of homogeneous two-dimensional turbulence](#). *J. Atmos. Sci.*, 29(2):394396, Mar 1972.
- [21] R. Ni and K.-Q. Xia. [Experimental investigation of pair dispersion with small initial separation in convective turbulent flows](#). *Phys. Rev. E*, 87(6), Jun 2013.
- [22] G. P. Bewley, E.-W. Saw, and E. Bodenschatz. [Observation of the sling effect](#). *New Journal of Physics*, 15(8):083051, Aug 2013.
- [23] A. Groisman and V. Steinberg. [Elastic turbulence in a polymer solution flow](#). *Nature*, 405(6782):53–55, May 2000.
- [24] R. G. Larson. [Fluid dynamics: Turbulence without inertia](#). *Nature*, 405(6782):2728, May 2000.
- [25] E. Afik. [Robust and highly performant ring detection algorithm for 3d particle tracking using 2d microscope imaging](#). *ArXiv e-prints*, Oct 2013. submitted.
- [26] P. K. Yeung and M. S. Borgas. [Relative dispersion in isotropic turbulence. part 1. direct numerical simulations and reynolds-number dependence](#). *J. Fluid Mech.*, 503:93–124, Mar 2004.
- [27] N. T. Ouellette, H. Xu, and E. Bodenschatz. [A quantitative study of three-dimensional lagrangian particle tracking algorithms](#). *Experiments in Fluids*, 40(2):301–313, 2006.
- [28] R. Bitane, H. Homann, and J. Bec. [Time scales of turbulent relative dispersion](#). *Phys. Rev. E*, 86(4), Oct 2012.
- [29] G. Falkovich and A. Frishman. [Single flow snapshot reveals the future and the past of pairs of particles in turbulence](#). *Physical Review Letters*, 110(21), May 2013.
- [30] Y. Liu, Y. Jun, and V. Steinberg. [Concentration dependence of the longest relaxation times of dilute and semi-dilute polymer solutions](#). *Journal of Rheology*, 53(5):1069–1085, 2009.

- [31] A. D. Straw and M. H. Dickinson. [Motmot, an open-source toolkit for realtime video acquisition and analysis](#). *Source Code Biol Med*, 4(1):5, 2009.
- [32] D. H. Kelley and N. T. Ouellette. [Using particle tracking to measure flow instabilities in an undergraduate laboratory experiment](#). *Am. J. Phys.*, 79(3):267, 2011.
- [33] E. Jones, T. Oliphant, P. Peterson, et al. [SciPy: Open source scientific tools for Python](#). <http://www.scipy.org/>, 2001–. [Online; accessed 2014-11-12].
- [34] L. Wasserman. *All of Nonparametric Statistics (Springer Texts in Statistics)*. Springer, 2007.
- [35] K. Ahnert and M. Abel. [Numerical differentiation of experimental data: local versus global methods](#). *Computer Physics Communications*, 177(10):764–774, Nov 2007.
- [36] N. Y. Krakauer and B. M. Fekete. [Are climate model simulations useful for forecasting precipitation trends? hindcast and synthetic-data experiments](#). *Environmental Research Letters*, 9(2):024009, Jan 2014.

Supporting figures

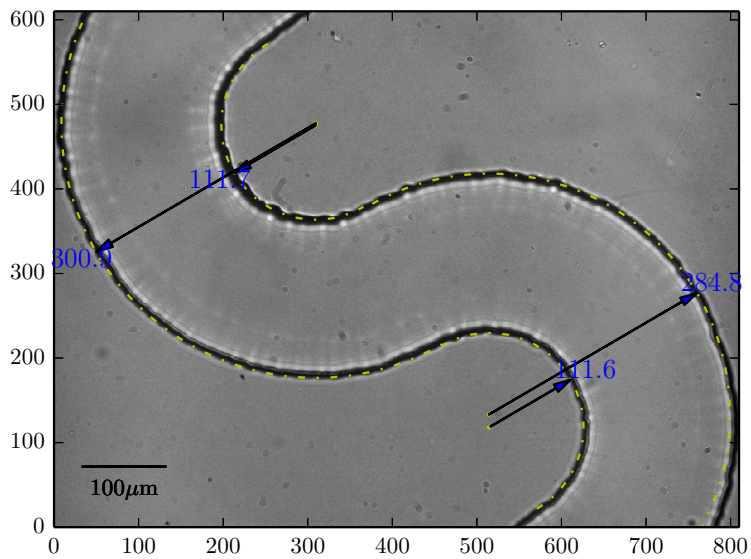


Figure S1: **Microfluidic tube geometry.** A bright field image of the observation window; the tube geometry is based on a planar concatenation of co-centric pairs of half circles; the observation window encloses two out of 33 in total; the arrows, and the yellow broken line indicate the tube walls and their dimensions, specified in microns; the tube has a rectangular cross-section of 140 μm depth (perpendicular to the image plane).

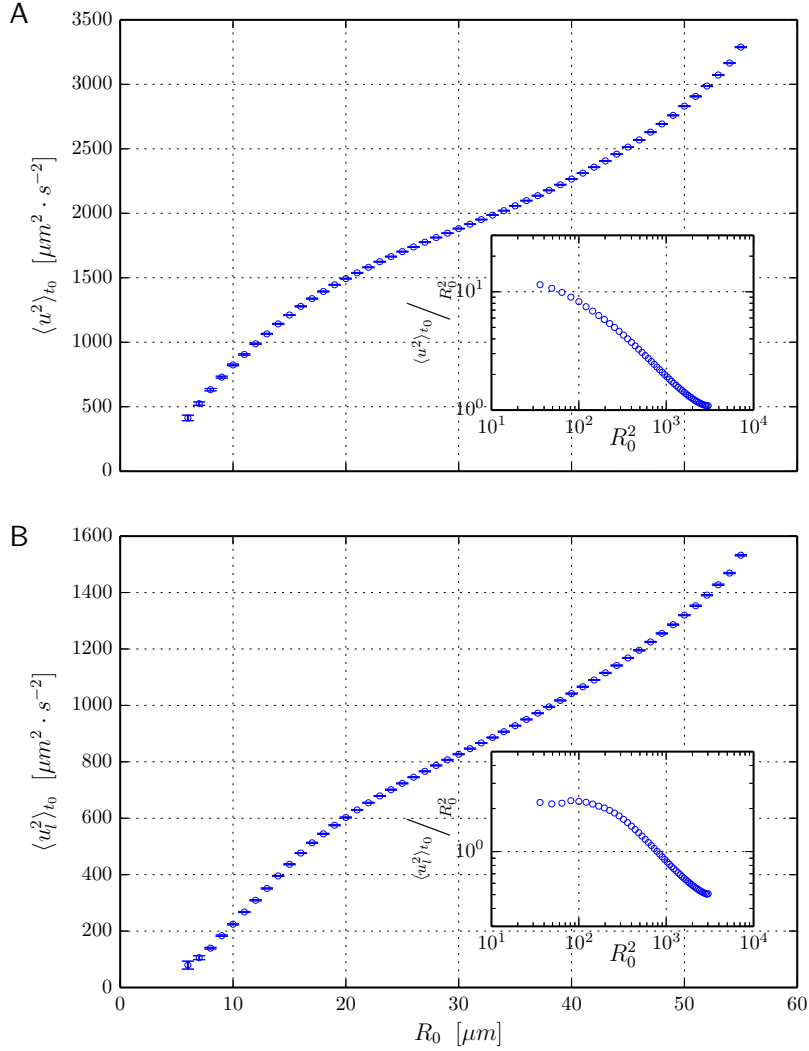


Figure S2: **Mean squared relative velocity at t_0 .** The averages are taken at t_0 , when the pairs separation distance is closest to R_0 , as function of R_0 , for: (A) squared relative velocity $\langle u^2 \rangle_{R_0, t_0}$, which is our estimator for the coefficient of the quadratic term in Eq. 5 (see the closing note of the Materials and Methods), and (B) squared relative separation velocity $\langle u_l^2 \rangle_{R_0, t_0}$, where $u_l = \mathbf{u} \cdot \mathbf{R}/R$.

The error bars indicate the margin of error based on the 95% confidence interval. The insets show the same data rescaled by the squared initial separation distance R_0^2 , plotted vs. R_0^2 . The $\langle u_l^2 \rangle_{R_0, t_0}/R_0^2$ data (inset of B) levels off as R_0 approaches the smaller distances, providing supporting evidence for the linearity of u_l with R at scales smaller than 12 μm .

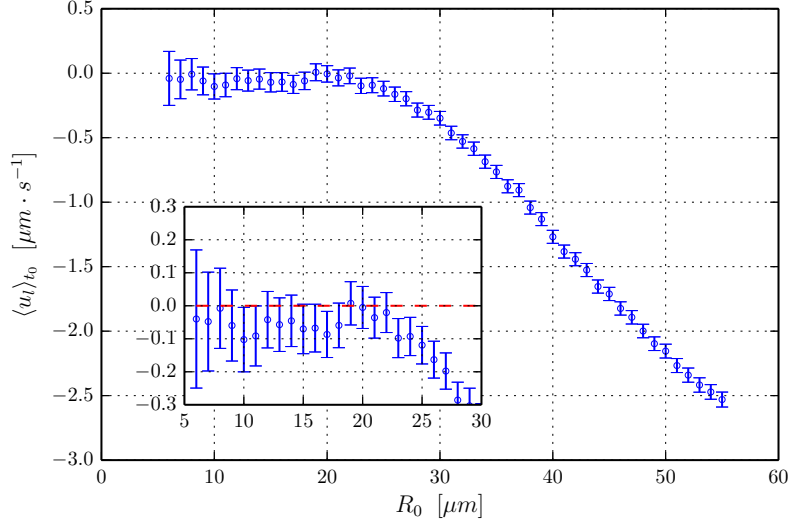


Figure S3: **Mean relative separation velocity at t_0 .** The averages are taken at t_0 , when the pairs separation distance is closest to R_0 , as function of R_0 , for the relative separation velocity $\langle u_l \rangle_{R_0, t_0}$. The error bars indicate the margin of error based on the 95% confidence interval. The inset shows a zoom-in on the smaller range of R_0 studied here, where $\langle u_l \rangle_{R_0, t_0}$ is nearly zero. This is an indication of a sampling with no preferential for pair trajectories which diverge or converge initially.

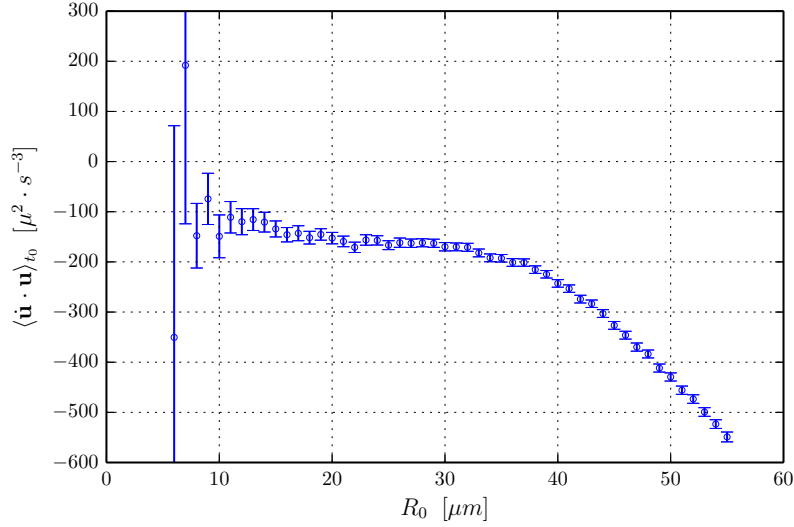


Figure S4: **The coefficient of the cubic term in Eq. 5, $\langle \dot{\mathbf{u}} \cdot \mathbf{u} \rangle_{R_0, t_0}$.** The averages are taken at t_0 , when the pairs separation distance is closest to R_0 , as function of R_0 , for $\langle \dot{\mathbf{u}} \cdot \mathbf{u} \rangle_{R_0, t_0}$. It is also an estimator for the time derivative of $\langle \frac{1}{2} u^2 \rangle_{R_0, t_0}$. The error bars indicate the margin of error based on the 95% confidence. Due to the extent of the margin of error for $R_0 \leq 10$ we did not use these values for the re-scaling in Fig. 4.

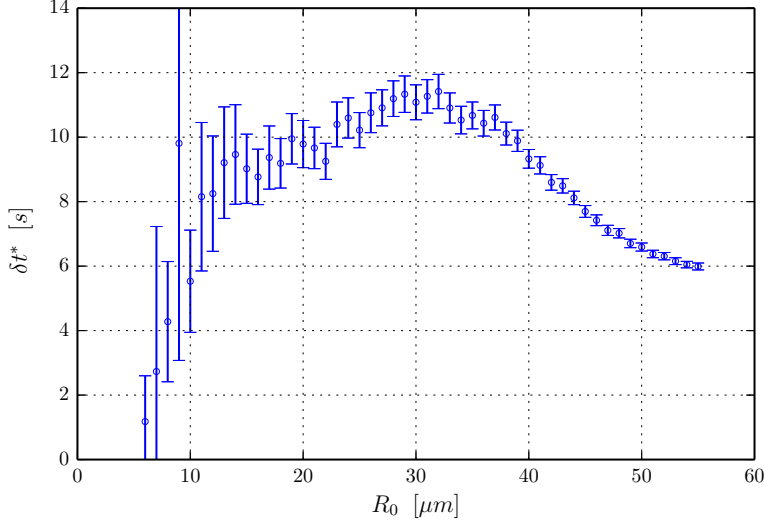


Figure S5: **Transition time from the ballistic regime.**

$\delta t_{R_0}^* = \left| \langle u^2 \rangle_{R_0, t_0} / \langle \dot{\mathbf{u}} \cdot \mathbf{u} \rangle_{R_0, t_0} \right|$ is plotted as function of the initial separation distance R_0 . Deviations of the relative dispersions $\langle \|\mathbf{R} - \mathbf{R}_0\|^2 \rangle_{R_0}$ from the δt^2 scaling are generically expected to be significant for $\delta t \gtrsim 0.1 \delta t^*$.

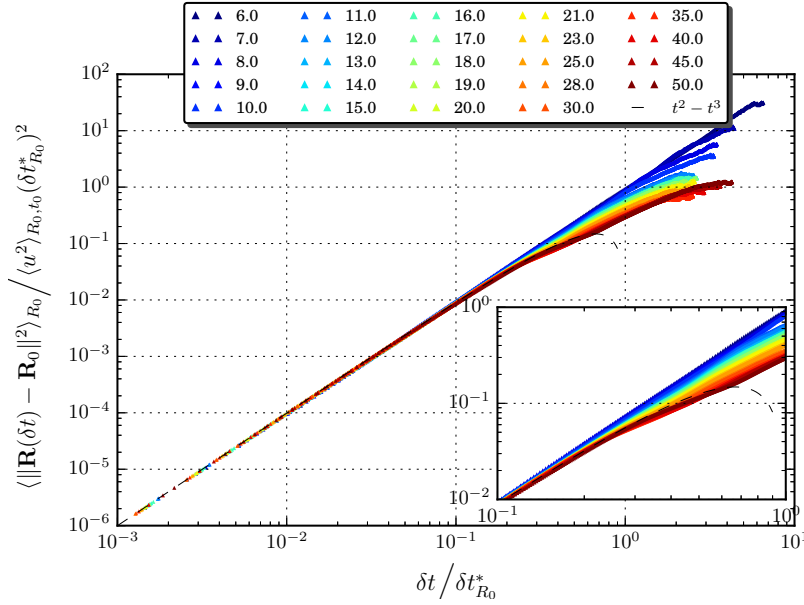


Figure S6: **Dimensionless relative pair dispersion.** The short-time statistics of the relative pair dispersion Eq. 5 is reformulated in a dimensionless form when divided through by $\langle u^2 \rangle_{R_0, t_0} (\delta t_{R_0}^*)^2$. The rescaled data, for various initial separations between 6 and 50 μm , is plotted in the figure against the dimensionless time $\delta t / \delta t_{R_0}^*$; here $\delta t_{R_0}^*$ is the same as plotted in Fig. S5. The datasets indeed collapse onto a single curve $(\delta t / \delta t_{R_0}^*)^2 - (\delta t / \delta t_{R_0}^*)^3$, shown by the dashed black line, for $\delta t / \delta t_{R_0}^* \lesssim 0.2$. As can be seen from the zoom-in (inset), the datasets of larger initial separations $R_0 \gtrsim 23 \mu\text{m}$ follow the short-time statistics more closely longer. The uncertainty of our estimator for $\delta t_{R_0}^*$ at smaller initial separations is larger, as reflected by the errorbars in Fig. S5; reducing the degree of the uncertainty may provide better understanding of why the data collapse is less pronounced for the smaller R_0 ensembles.

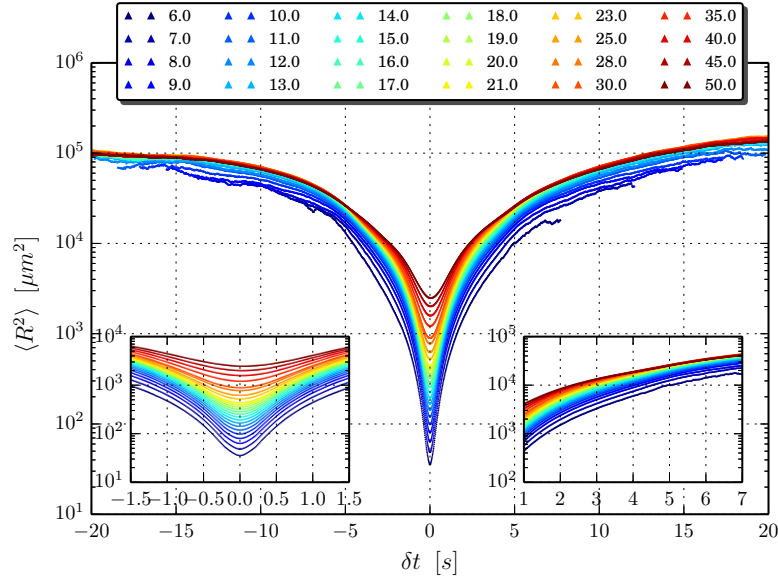


Figure S7: **Pair dispersion.** The plot shows the average squared pair separation distance, $\langle R^2 \rangle_{R_0}$ for various R_0 between 6 and 30 μm ; the insets show a zoom-in on the initial and intermediate time intervals. This is the same data plotted in Fig. 2, only not normalised by R_0 .

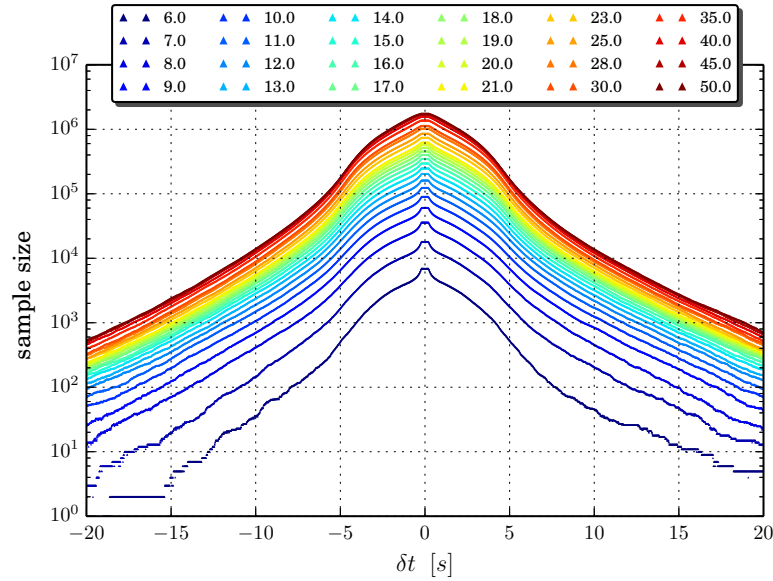


Figure S8: **Sample sizes.** The number of pairs in the datasets presented in this work plotted against δt for the various initial separation distances R_0 . These sample sizes result from several filters on the observed pairs: each single trajectory is required to span more than 140 μm ; every $R(t)$ trajectory is let to contribute to an R_0 bin at most once, at the point where it is nearest to the centre of the bin, this moment is denoted t_0 for the pair in this bin; the pair trajectory is required to contain at least 15 measurement points before and after t_0 . Averages of sample sizes smaller than 100 were excluded.